Experimental and Theoretical Charge Density Analysis of a Bromoethyl Sulfonium Salt

ARTICLE *in* THE JOURNAL OF PHYSICAL CHEMISTRY A · NOVEMBER 2013

Impact Factor: 2.69 · DOI: 10.1021/jp410301d · Source: PubMed

6 AUTHORS, INCLUDING:

Maqsood Ahmed
The Islamia University of Bahawalpur
18 PUBLICATIONS **45** CITATIONS
SEE PROFILE

Muhammad Yar
COMSATS Institute of Information Technology
47 PUBLICATIONS **259** CITATIONS
SEE PROFILE

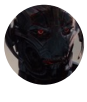

Benoit Guillot
University of Lorraine
76 PUBLICATIONS **759** CITATIONS
SEE PROFILE

Christian Jelsch
French National Centre for Scientific Research
129 PUBLICATIONS **1,997** CITATIONS
SEE PROFILE

THE JOURNAL OF PHYSICAL CHEMISTRY A

Article

pubs.acs.org/JPCA

Experimental and Theoretical Charge Density Analysis of a Bromoethyl Sulfonium Salt

Maqsood Ahmed,[†,‡] Muhammad Yar,[§] Ayoub Nassour,[†] Benoit Guillot,[†] Claude Lecomte,[†] and Christian Jelsch*[,†]

[†]CRM2, CNRS-Institut Jean Barriol, Université de Lorraine, Vandoeuvre-lès-Nancy, France

[‡]Department of Chemistry, The Islamia University of Bahawalpur, Bahawalpur, Punjab, Pakistan

[§]Interdisciplinary Research Center in Biomedical Materials, COMSATS Institute of Information Technology, 54000, Lahore, Pakistan

Supporting Information

ABSTRACT: Bromoethyl sulfonium trifluoromethanesulfonate is a salt complex in which a sulfur atom makes three covalent bonds. This molecule has been proved to act as an efficient annulation reagent which results in formation of synthetically challenging and pharmaceutically important 4-, 5-, 6-, and 7-membered heterocycles in excellent yields. The charge density of the molecule was determined from both experimentally and theoretically derived diffraction data. The stereochemistry and electron density topology of the sulfonium group was analyzed. To understand the chemical reactivity of the molecule, the electrostatic potential difference between the two carbon atoms of the bromoethyl group was investigated. It has been considered that the hydrogen atoms on the carbon atom bound to sulfur are more acidic in character due to their vicinity with the triply covalently bonded positively charged sulfur atom. The electropositivity of the S-attached and Br-attached methylene groups are compared in the experimental and theoretical charge densities using topological atomic charges and electrostatic potential at the molecular surface.

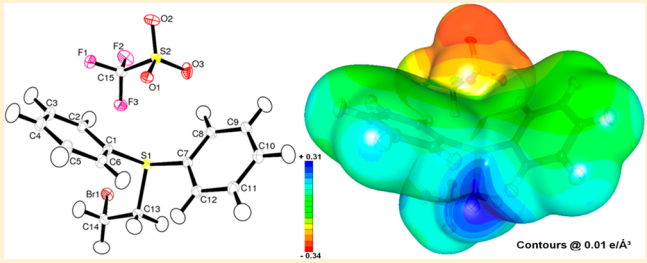

INTRODUCTION

Bromoethyl sulfonium triflate **1** (or BEST, Scheme 1) has been found to be an effective annulation reagent in the synthesis of various medicinally important compounds.[1−7] Diphenylvinylsulfonium triflate **2** (or DVST, Scheme 1) has been extensively used and found to be very reactive toward various nucleophiles. A variety of nitrogen-, sulfur-, oxygen-, and carbon-based nucleophile molecules undergo conjugate addition to vinyl sulfonium salts in the presence of base;[3,5,8] the resulting ylide has two possible reaction pathways depending upon the substrates type. In a first reaction type, the resulting ylides can be trapped intra- or intermolecularly by aldehydes or imines to produce epoxides or aziridines, respectively.[1,2,5,9] In another reaction type, ylides undergo intramolecular proton transfer from an acidic site and the anion generated then displaces the sulfide to effect a ring closure to generate required heterocycles.[7,10]

Scheme 1. Chemical Diagram of Bromoethyl Sulfonium Trifluoromethanesulfonate 1 (BEST) and Diphenylvinylsulfonium Triflate 2 (DVST)

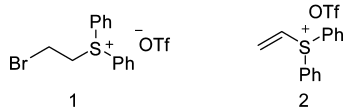

DVST is a good alternative of 1,2-dihaloethanes for synthesis of heterocycles. 1,2-Dihalo derivatives are less reactive toward nucelophiles, and their reactions usually give unwanted side products. For example, direct synthesis of 1,4-diheterocyclic compounds by alkylation of β-amino alcohols/thiols/amines with 1,2-dihaloethanes often gives low yields and side reactions.[11] DVST (soft electrophile, good Michael acceptor) operates under less basic conditions and minimizes competing elimination pathways. Thus, the efficient synthetic procedure for DVST and its synthetic applications has made it an attractive annulation agent.

It was later discovered that these annulations can be conducted using BEST compound **2**, which possibly generates diphenylvinylsulfonium triflate in situ. BEST is a crystalline solid and easier to handle and store as compared to dense liquid DVST.[4] BEST works effectively with a modification of the nature of the base; this method gave access to a range of heterocycles in high yields (Scheme 2). The range of nitrogen substituents demonstrated to be suitable was expanded to include sulfinamides, *N*-aromatics, and *N*-heteroaromatic substituents.[4,6] Concerning the challenging synthesis of seven-membered heterocycles (diazepines and oxazepines), the

Received: October 17, 2013
Revised: November 18, 2013
Published: November 28, 2013

   dx.doi.org/10.1021/jp410301d | J. Phys. Chem. A 2013, 117, 14267−14275

Scheme 2. Schematic Illustration of Reactions Involving BEST To Give Various Heterocycles

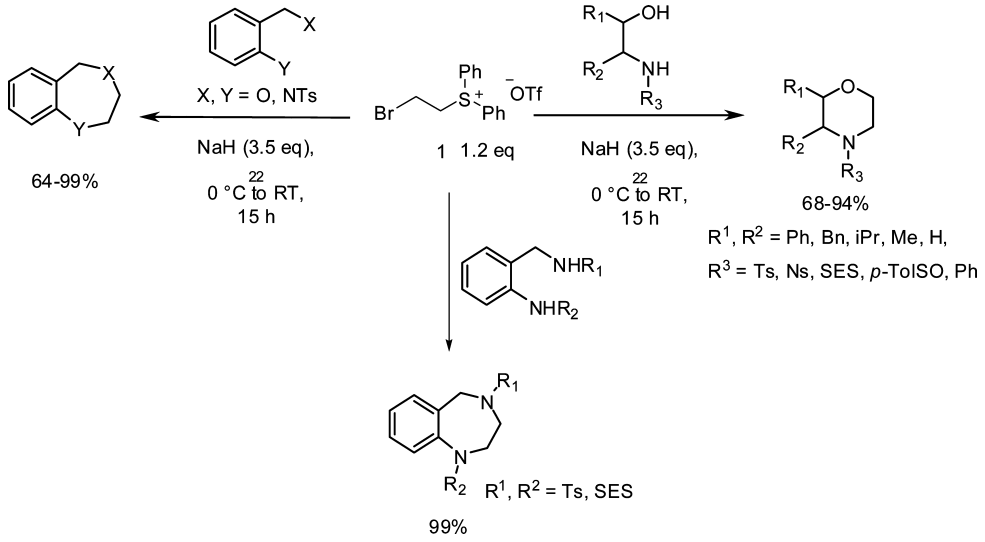

Scheme 3. Reported Proposed Mechanism of Annulation Reaction Involving BEST (see references above)

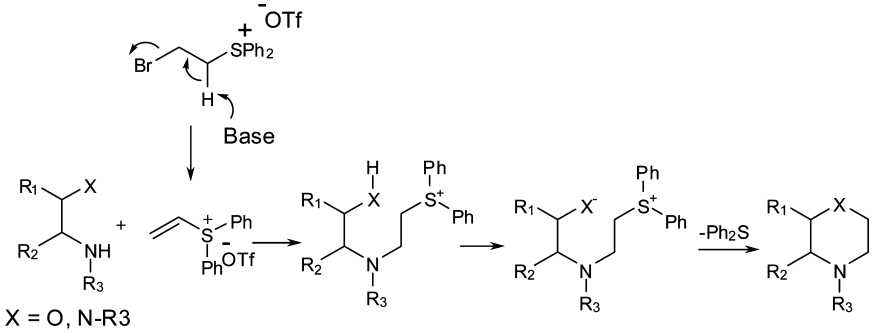

annulation reaction of 1,3-aminoalcohols and 1,3-diamines with BEST gave 7-membered ring heterocycles in good yield.[4] Employing *N*-tosyl 1,3-amino alcohols or 1,3-diamines and bromoethyl sulfonium salt yielded 1,4-oxazepines or 1,4-diazepines, respectively, in moderate to excellent yields. A mixed *N*-tosyl/*N*-SES 1,3-diamine gave a heterocycle in good yield which can be deprotected and derivatized as required.

When BEST is employed in the transformations described above a plausible mechanism could be successive S_N2 displacements of diphenylsulfide and -bromide. It has been suggested that the reaction proceeds through in situ formation of DVST followed by conjugate addition as shown in Scheme 3.[1−5]

As the reactivity of a compound such as BEST is related to its electron distribution, a precise charge density analysis (either experimental or theoretical) is a method of choice to recover molecular properties. In particular, it is of interest to know how the two CH_2 carbon units present in compound BEST between the bromine and the sulfur atom are different from a charge distribution point of view. It has been assumed[4] that the carbon atom attached to the sulfur atom is probably more electron deficient due to the positive charge of S and hence would be the site of attack by a base, owing to its comparatively acidic hydrogen atoms (Scheme 4).

To test this hypothesis, an experimental (Exp) and theoretical (Theo) charge density determination on bromoethyl sulfonium trifluoromethanesulfonate **1** (BEST) was carried out.

Scheme 4. Proposed[4] Distribution of Charges on C13 and C14 Atoms in BEST Compound

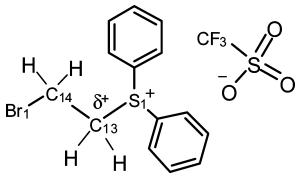

MATERIALS AND METHODS

Crystallization. Synthesis of the BEST compound was described before.[3−5,12] Being an organic salt, the compound crystallizes very easily in a number of solvents including alcohols, acetone, and chloroform. For the current experiment, crystals were grown by slow evaporation of a toluene solution of BEST compound in a few days at room temperature. A single, colorless crystal of dimensions 0.18 × 0.16 × 0.15 mm was selected for the diffraction experiment.

Data Collection. Single-crystal X-ray high-resolution and highly redundant data collection of BEST was performed on an Oxford SuperNova[13] diffractometer using Mo Kα radiation (λ = 0.71073 Å). Details of the data collection and refinement procedure are given in Table 1. The crystal was mounted on a glass needle using silicone grease and cooled from room temperature to 100(1) K over a period of 1 h under a stream of liquid nitrogen using the Oxford Cryo-systems gas flow

dx.doi.org/10.1021/jp410301d | J. Phys. Chem. A 2013, 117, 14267−14275

Table 1. Crystal and Data Collection Statistics

chemical formula	$C_{15}H_{14}BrF_3O_3S_2$
molecular weight (g/mol)	443.29
space group	monoclinic $P2_1/n$
temperature (K)	100 (1)
a, *b*, *c* (Å)	11.7897(8), 10.5840(6), 13.6153(6)
β (deg)	97.989(10)
radiation type	Mo Kα
cryst shape	prism, colorless
cryst dimens (mm)	0.18 × 0.16 × 0.15
diffractometer	Oxford SuperNova
abs corr	Analytical (Clark and Reid, 1995)
μ (mm^{-1})	2.737
T_{min}, T_{max}	0.648, 0.795
sin θ_{max}/λ	1.02
no. of measd, independent reflns	679 441, 15 489
no. of used reflns	14 538 ($I > 0\sigma$)
completeness (%)	99.9
R_{int} %/redundancy	5.7/35

apparatus. The SuperNova diffractometer works under the software CrysAlisPro,[13] which calculates the strategy to optimize the angular positions of detector and the goniometer head during data collection.

A first diffraction data set was collected under ω scans of 1° intervals. To improve the quality of the data a second data set was later collected using the same crystal at the same temperature but using different exposure times in the experiment. In the first experiment, the exposure time was 10 and 25 s for low- and high-resolution data. In the second experiment, a 45 s exposure time was used for high-angle data collection whereas the low-angle data were also collected at the 10 s exposure time. Image frames were indexed and integrated using the CrysalisPro package. An analytical absorption correction[14] was applied on the basis of the face indexes of the crystal. Friedel mates were merged during data processing, the crystal being centrosymmetric space group $P2_1/n$. Two data sets were then merged using SORTAV.[15] Although intensity peaks were observed up to d = 0.44 Å resolution, data resolution was truncated at d > 0.50 Å as the very high resolution reflections were very weak and the $\langle I_{obs}\rangle/\langle I_{calcd}\rangle$ ratio became significantly larger than unity (reaching 1.16) as verified with XDRKplot[16] software (see Supporting Information).

Structure Solution and Refinement. The structure was solved in the monoclinic $P2_1/n$ space group using the SIR92[17] software. An initial Independent Atom Model (IAM) refinement was undertaken using the SHELXL97 software.[18] The model was subsequently imported to MoPro[19] software. Hydrogen atom positions were constrained to the standard neutron distances as available in the *International Tables of Crystallography*.[21] The bromine atom was modeled using an anharmonic thermal motion description up to fourth order of Gram–Charlier parameters; the resulting ⟨root-mean-square⟩/⟨sigma⟩ ratio is 7.0. An ORTEP[22] diagram of the molecule showing the atom-numbering scheme and thermal ellipsoids is shown in Figure 1.

Fourier residual electron density maps obtained after experimental IAM refinement are shown in the Supporting Information. Examination of these maps demonstrate the quality of the experimental data, as deformation bonding electron densities can be found on all covalent bonds, as well as around atoms holding electron lone pairs (S, Br). Crystallographic statistics are given in Table 2.

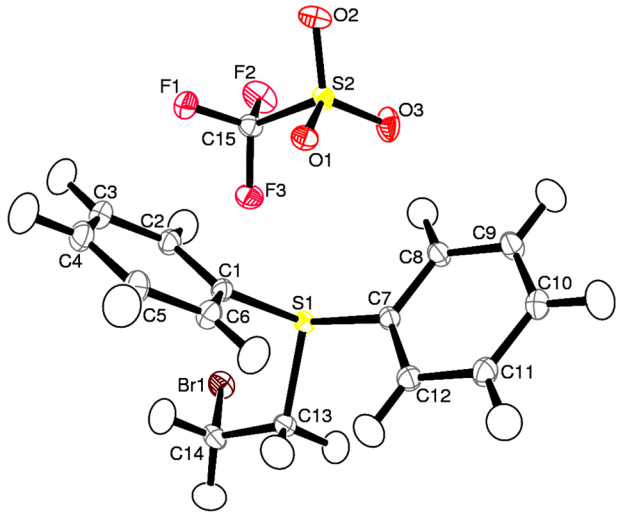

Figure 1. ORTEP diagram of the molecule showing the atom-numbering scheme and thermal displacement ellipsoids, drawn at the 50% probability level.

Table 2. Crystallographic Agreement Factors and Residual Electron Density Values Obtained after Multipolar Refinements of the BEST Molecule

data	Exp	DFT DZP
resolution (Å)	0.50	0.40
$R(F)$ %	1.68	1.10
$wR_2(F)$ %	1.15	1.07
Gof	0.99	
$\Delta\rho_{max}$ (e/Å^3)	0.36	
$\Delta\rho_{min}$	−0.41	
$\Delta\rho_{rms}$	0.055	

Experimental Multipolar Refinement. The least-squares multipole refinement was carried out with MoPro software[19] on the basis of the Hansen and Coppens[20] model. Parameters of the Slater radial functions used for the multipolar description of atoms are given in Table Sup3, Supporting Information. Reflections up to d = 0.50 Å resolution and with $I > 3\sigma$ were used in the refinement. The different structural and charge density parameters were refined iteratively. Coordinates and thermal displacement parameters of all non-hydrogen atoms were refined using high-order diffraction data only (d <0.7 Å) in the initial stages of the refinement. After a first round of charge density refinement anisotropic thermal displacement parameters of H atoms were calculated with the SHADE server[29] and were kept fixed subsequently.

Constraints and Restraints. C–H covalent bonds were restrained to standard neutron distances[21] (σ_d = 0.002 Å). Target C–H distances were 1.083(2) Å for aromatic groups, 1.059(2) Å for the bromomethyl group, and 1.092(2) Å for the methylene group.

The following restraints were applied in the experimental charge density refinement. κ parameters of all H atoms were restrained to 1.16 (0.01).[30]

R-free refinements were performed to estimate the best weight to be applied to the chemical equivalence and multipoles local symmetry restraints.[31] The sigma value σ_r =

dx.doi.org/10.1021/jp410301d | J. Phys. Chem. A 2013, 117, 14267–14275

0.02 was found to be optimal as it gave the lowest values of $wR^2(F)$ free factor (Figure Sup4, Supporting Information). A mirror symmetry restraint was imposed on the S1 atom as it is linked to two sp^2 and one sp^3 carbon atoms. A *3m* symmetry restraint was imposed on the triflate S2 atom ($C-SO_3^-$ type) (see Figure 1). Similarly, *3m* symmetry was imposed on atom C15 bearing the three fluorine atoms. All other carbon atoms had one single mirror symmetry. Charge density parameters of the chemically equivalent atoms were restrained to be similar with the same sigma value σ_r. Two ions forming the asymmetric unit were constrained to have a formal charge of ±1.

It was observed that the multipolar refinement did not allow reaching a proper charge distribution model for the three fluorine and oxygen atoms of the triflate anion. This was probably due to the higher thermal motion within the triflate which has a rotation degree of freedom around the S−C axis and the F2 atom has a U_{eq} value reaching 0.03 Å^2. Chemical equivalence constraints were therefore applied to the three fluorine and oxygen atoms, which yielded realistic experimental deformation electron density.

At the end of the multipolar refinement against the experimental data, the R (F) factor was 1.68% and the goodness of fit was 0.99. All fractional coordinates, bonds lengths, bond angles, and thermal displacement parameters are listed in the CIF file in the Supporting Information.

Theoretical Calculations. The CRYSTAL09[22] program package was used to perform periodic quantum mechanical calculations. The crystal geometry observed experimentally was used as a starting geometry, and optimization of the hydrogen-atom positions was performed with the density functional theory (DFT) method[23] and the B3LYP hybrid functional[24,25] using 6-31G(d,p) basis set.[27] Upon convergence on energy ($\Delta E \approx 10^{-6}$) the periodic wave function based on the optimized geometry was obtained. The index generation scheme proposed by Le Page and Gabe[28]was applied to generate 27 520 unique Miller indices up to sin θ/λ = 1.25 Å^{-1}. The option XFAC of the CRYSTAL09 program was then used to generate a set of theoretical structure factors from the computed electron density using the set of prepared indices.

Structure factors were calculated and taken as the observed data set in a subsequent refinement of the charge density parameters with the software MoPro. For the non-H atoms, a κ coefficient applying to the core electron density was in addition refined, as performed previously in a charge density analysis of corrundum[32]

RESULTS AND DISCUSSIONS

Electron Density. Some static deformation and the corresponding residual electron density maps obtained at the end of the multipole refinement against experimental data are shown in Supporting Information. Fourier residual electron density maps are almost featureless (Table 2). A three-dimensional view of the static deformation electron density around the S1 atom is shown in Figure 2. An electron lone pair is visible on the S1 sulfur atom and forms a tetrahedral geometry with the three C−S bonds. The sulfonate S2 atom of the triflate anion has a different configuration as it is bonded with three oxygen atoms and one carbon atom and is arranged in a nearly tetrahedral geometry (Figure 1).

Bond Critical Points. Covalent bond critical points (BCP) were searched and are shown in Figure 3, while the topological properties are listed in Tables 3 and Sup1, Supporting Information. It can be observed in Table Sup1, Supporting

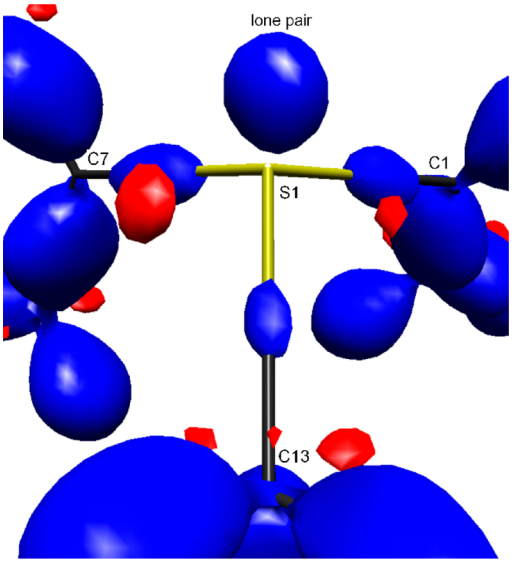

Figure 2. 3D view of the experimental static deformation electron density showing the electron lone pair of the sulfur atom. Blue color shows deformation electron density accumulation, and red color shows depletion. Isosurfaces levels are ±0.2 e·Å^{-3}.

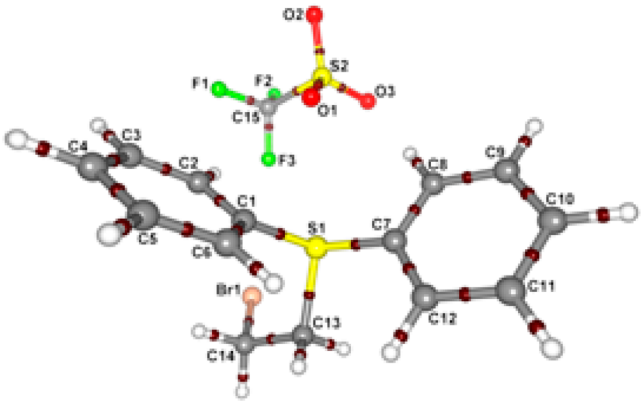

Figure 3. Covalent bond critical points shown in dark brown color for the experimental model.

Information, that the topological values from experiment and theory are in general agreement with each other.

The $\nabla^2\rho_{cp}$ values of the Laplacian at the BCPs are found to be negative except on the sulfonate S−O bonds and on the C−Br bond. This is the case for both experimental and theoretical cases and denotes the polar character of these bonds. A negative minimum of the Laplacian is however found on the C−O bond path to the oxygen atoms and on the C−Br bond closer to the electronegative Br atom (Figure 4). The values of the ellipticity on the S−O bonds are small (0.03 ± 3 on average) and reflect the nearly 3-fold symmetry character of the $O-SO_2C$ bonds; the three S−O distances are very similar at 1.446 ± 5 Å.

The negative Laplacian is stronger on the triflate S2−C15 BCP than on the S1−C BCPs of the sulfonium, despite a longer bond length for S2−C15 (1.8320(5) vs 1.79 ± 2 Å). The same tendency is observed for the Theo charge density. Contrary to nonpolar bonds, the Laplacian $\nabla^2\rho_{cp}$ cannot be directly related to the bond strength in polar bonds such as S−C or S−O. This result can be related to the experimental charge density study of K_2 sulfate,[34] where the longest S−O bonds also

dx.doi.org/10.1021/jp410301d | J. Phys. Chem. A 2013, 117, 14267−14275

Table 3. Topological Properties at the Bond Critical Points in the Bromoethyl Sulfonium and Triflate Parts of the BEST Molecule (experimental multipolar model)[a]

bond	d_{12}	$d_{1\ cP}$	$d_{2\ cP}$	$\rho(r_{cp})$	$\nabla^2\rho(r_{cp})$	ε
BR1−C14	1.9458(6)	1.0948	0.8513	0.9662	0.03	0.01
S1−C1	1.7823(5)	0.9493	0.8330	1.2739	−5.7	0.05
S1−C7	1.7796(5)	0.9508	0.8291	1.2880	−5.5	0.04
S1−C13	1.8158(5)	0.9785	0.8372	1.1891	−4.5	0.08
C13−C14	1.5126(7)	0.7855	0.7278	1.6641	−10.2	0.04
C13−H13A	1.0907	0.7393	0.3515	1.7932	−15.9	0.00
C13−H13B	1.0914	0.7309	0.3606	1.7418	−14.9	0.00
C14−H14A	1.0914	0.7338	0.3577	1.8048	−16.5	0.01
C14−H14B	1.0919	0.7308	0.3611	1.7789	−15.9	0.01
S2−C15	1.8320(6)	0.8981	0.9341	1.3348	−9.2	0.02
S2−O1	1.4508(8)	0.5918	0.8591	2.1894	3.3	0.06
S2−O2	1.4467(9)	0.5921	0.8552	2.1741	3.8	0.01
S2−O3	1.4410(9)	0.5924	0.8503	2.2165	3.8	0.01
F1−C15	1.3415(6)	0.8238	0.5180	1.9470	−15.6	0.05
F2−C15	1.3334(7)	0.8263	0.5074	1.9328	−13.9	0.06
F3−C15	1.3340(6)	0.8236	0.5109	1.9784	−16.2	0.07

[a] d_{12} is the interatomic distance, $d_{1\ cP}$ and $d_{2\ cP}$ (Å) is the distance between the first/second atom and the CP; $\rho(r_{cp})$ is the total electron density (e·Å^{-3}); $\nabla^2\rho(r_{cp})$ is the Laplacian (e·Å^{-5}); ε is the ellipticity. Values are from the experimental model. Other BCPs and values from theory are described in the Supporting Information.

have the strongest $\nabla^2\rho_{cp}$ Laplacian values. When the S−O distance is decreased in sulfate, the S−O bond unexpectedly becomes less covalent because of a counterbalancing effect arising from the large enhancement of the bond polarity. In theoretical studies of S−O and N−O polar covalent bonds in several small molecules in vacuo, Love[35,36] found however that the Laplacian $\nabla^2\rho_{cp}$ is generally decreasing in magnitude when the bond length increases.

It can also be noticed that the BCP is closer to the carbon atom in the sulfonium C−S bonds, while the reverse occurs in the triflate C−S bond, denoting the stronger electron depletion of the sulfonate S atom. The three sulfonium S−C bonds have ellipticities of 0.06 ± 2, and the S1−C13 bond involving a sp^3 C atom is slightly longer than the two others which involve aromatic C atoms (Table 3).

Values of ellipticity for the aromatic C(sp^2)−C(sp^2) bonds on the phenyl rings are higher which is related to the partial double-bond character. The average value is ε = 0.20 ± 2 and 0.16 ± 2 for the 12 C−C covalent bonds found in the two phenyl rings for the Exp and Theo models, respectively.

Intermolecular Interactions. There is a large number of intermolecular interactions of different nature present in the crystal structure. The Hirshfeld surface analysis was performed with the program CRYSTALEXPLORER[38] to find out the respective proportions of the various interactions. A Hirshfeld surface[39] of the molecule (Figure Sup6, Supporting Information) shows the areas where intermolecular interactions are shorter than the sum of atomic van der Waals radii.

The "fingerprint" plots of the interactions are shown in the Supporting Information, and a breakdown of the interaction surfaces is listed in Table 4. The H···O hydrogen bonds constitute the largest contact area, followed by H···H, H···F, and H···C interactions. H···Br interactions are present in a significant ratio of 10.6%. A small but interesting proportion of interactions of Br···F type is also observed, although the bromine and F2 atoms are distant by more than 3.45 Å in the crystal packing.

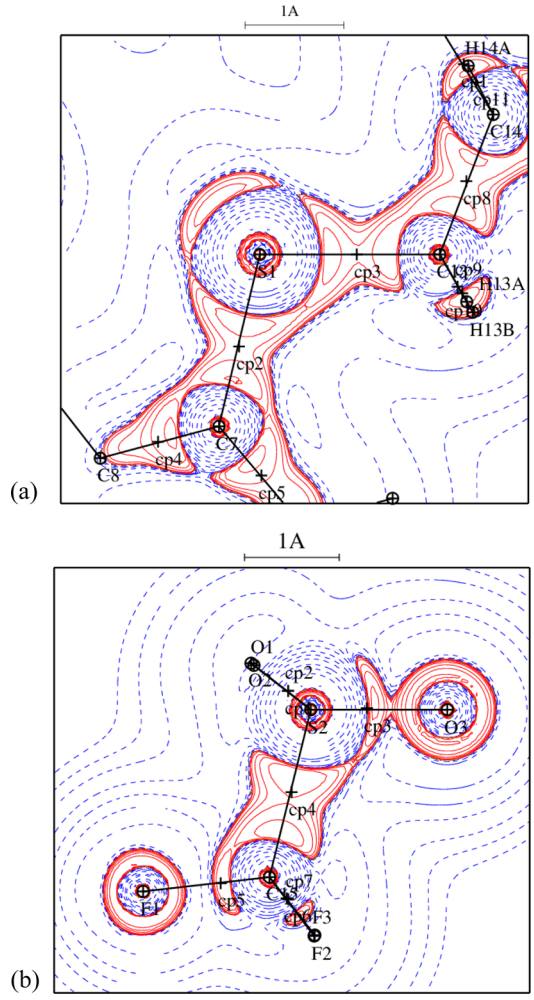

Figure 4. Electron density Laplacian $\nabla^2\rho$ maps of the experimental multipolar model: (a) in the C14−S1−C7 sulfonium plane; (b) in the C15−S2−O3 plane of the triflate anion.

Table 4. Breakdown of the Most Prevalent (>1%) Intermolecular Interactions in the BEST Crystal Packing with Their Respective Proportions

contacts	%	contacts	%
H···O	23.2	H···Br	10.6
H···H	20.8	C···F	6.7
H···F	19.5	Br···F	1.7
H···C	14.3	C···O	1.5

A topological analysis of the total electron density in the intermolecular interactions regions on the basis of Bader theory[35] of Atoms In Molecules (AIM) is a very informative way to study the nature of interactions. A topological analysis was performed for all significant and weak interactions in the crystal packing, and the intermolecular CPs were located. Topological values for all (3,−1)-type interactions are listed in Table Sup2, Supporting Information.

There are only C−H···O-type hydrogen bonds in the crystal packing of BEST compound, and those with a H···O distance

dx.doi.org/10.1021/jp410301d | J. Phys. Chem. A 2013, 117, 14267−14275

Table 5. Selection of Hydrogen Bonds and Their Topological Properties at the CP for the Experimental Model[a]

bond path	d_{12}	$d_{1\ cP}$	$d_{2\ cP}$	ρ	$\nabla^2\rho$	ε	G	V
O1···H6 (iv)	2.396	1.465	0.969	0.068	1.08	0.43	23.1	−16.9
O1···H13B (iv)	2.738	1.625	1.130	0.021	0.44	0.37	8.4	−4.95
O1···H12 (iv)	2.311	1.403	0.932	0.066	1.17	0.01	24.7	−17.4
O2···H4 (v)	2.661	1.539	1.164	0.042	0.63	0.13	13.0	−8.87
O2···H10 (iii)	2.692	1.617	1.085	0.021	0.48	0.16	9.2	−5.53
O2···H14B (i)	2.483	1.469	1.037	0.044	0.77	0.06	15.7	−10.4
O3···H13A (ii)	2.151	1.290	0.877	0.107	1.72	0.03	38.8	−30.8
F2···H9 (vi)	2.675	1.495	1.210	0.027	0.48	0.27	9.5	−5.88
F1···H10 (vi)	2.667	1.480	1.212	0.037	0.62	0.07	12.5	−8.19

[a]Definitions are in Table 3. G and V are the kinetic and potential energy density at the CP (kJ/mol/bohr^3). Symmetry codes are as follows: (i) $X, Y - 1, Z$; (ii) $-X + 1, -Y, -Z + 1$; (iii) $X + 1/2, -Y - 1/2, Z - 1/2$; (iv) $-X + 3/2, Y - 1/2, -Z + 3/2$; (v) $X - 1/2, -Y - 1/2, Z - 1/2$; (vi) $X + 1/2, -Y - 1/2, Z - 1/2$.

Table 6. Valence Populations P_{val_κ} Derived from the Kappa Refinements and P_{AIM} Derived from Topology Using Experimental (Exp) and Theoretical (Theo) Models[a]

atom	P_{val_κ} Exp	P_{AIM} Exp	P_{val_κ} Theo	P_{AIM} Theo	atom	P_{val_κ} Exp	P_{AIM} Exp	P_{val_κ} Theo	P_{AIM} Theo
F1	7.11(2)	7.58	7.22(1)	7.57	Br1	6.57(8)	7.04	7.37(3)	7.44
F2	=F1	7.57	7.22(1)	7.61	O1	6.48(2)	7.27	6.53(1)	7.33
F3	=F1	7.59	7.22(1)	7.62	O2	=O1	7.27	6.53(1)	7.31
S1	5.38(6)	5.50	5.62(3)	5.69	O3	=O1	7.26	6.53(1)	7.35
S2	5.50(7)	2.86	5.25(3)	2.26	C8	4.23(6)	4.04	4.15(3)	3.92
C1	4.26(6)	4.14	4.10(3)	4.11	C9	4.21(7)	4.09	4.14(3)	3.95
C2	4.34(6)	4.03	4.18(3)	3.89	C10	4.21(6)	4.15	4.16(3)	3.97
C3	4.17(7)	4.09	4.19(3)	3.96	C11	4.08(7)	4.13	4.18(3)	3.92
C4	4.28(6)	4.23	4.17(3)	3.96	C12	4.27(6)	4.03	4.12(3)	3.91
C5	4.21(7)	4.04	4.17(3)	3.94	**C13**	**4.20(6)**	**4.24**	**4.35(3)**	**3.96**
C6	4.16(6)	4.12	4.19(3)	3.94	**C14**	**4.41(7)**	**4.13**	**4.12(3)**	**3.92**
C7	4.16(6)	4.14	4.10(3)	4.10	C15	3.73(6)	2.59	3.48(2)	2.96
H2	0.77(2)	0.86	0.77(1)	0.99	H10	0.77(2)	0.87	0.78(1)	0.95
H3	0.80(2)	0.85	0.78(1)	0.97	H11	0.83(2)	0.86	0.76(1)	0.97
H4	0.75(2)	0.83	0.77(1)	0.93	H12	0.79(2)	0.80	0.77(1)	0.97
H5	0.78(2)	0.85	0.76(1)	0.95	**H13A**	**0.81(2)**	**0.83**	**0.74(1)**	**0.93**
H6	0.75(2)	0.82	0.76(1)	0.98	**H13B**	**0.79(2)**	**0.86**	**0.75(1)**	**0.96**
H8	0.74(2)	0.85	0.76(1)	0.97	**H14A**	**0.77(2)**	**0.84**	**0.77(1)**	**0.94**
H9	0.77(2)	0.87	0.76(1)	0.99	**H14B**	**0.74(2)**	**0.85**	**0.76(1)**	**0.90**
methylene charge									
C13	+0.20	+0.06	+0.16	+0.15					
C14	+0.08	+0.18	+0.35	+0.24					

[a]$P_{AIM} = Q_{AIM} - N_{cor}$ is the number of electrons Q_{AIM} integrated over the Bader atomic basins (multipolar models) minus N_{cor}, the number of core electrons. Atomic charges can be retrieved by difference $N_{val} - P_{val}$ with the number of valence electrons N_{val} of the neutral atom. N_{val} = 7, 6, 7, 6, 4, 1e for Br, S, F, O, C, and H, and $N_{val} + N_{cor} = Z$, the atomic number.

significantly below the van der Waals contact distance are reported in Table 5. Topological values reveal that some of the interactions are remarkably strong. For example, the O3^{i}···H13A−C13 hydrogen bond has very high electron density and Laplacian values at the CP. The 2.155 Å O···H distance (Exp model) is quite short for a C−H···O-type weak hydrogen bond[38] and represents a significant interpenetration of atoms beneath van der Waals contact (d = 2.61 Å). The oxygen atom O3 on the $-SO_3^-$ group is a strong acceptor, while H bonds are shorter when the H−C donors are acidic; this is the case for H13A as its electrons are withdrawn by the nearby sulfonium atom.

The sulfonium S1 atom shows no intermolecular CP, although it is in contact with the sulfonate O3 atom at 3.169(1) Å, which is a distance below the van der Waals contact.

There 5, 6, and 7 critical points related, respectively, to H···H, H···F, and H···C interactions (Table Sup2, Supporting Information).

Atomic Charges. On the basis of the multipolar refinement result, analysis of the valence populations was made, as atomic charges can be derived from them. The kappa refinement formalism[33] was considered to avoid the possible charge transfers between atoms due to the multipoles in the Hansen and Coppens modeling. The valence populations P_{val_κ} results of the kappa refinements are mentioned in Table 6.

The Bader Quantum Theory of Atoms in the Molecules (QTAIM)[34] provides another reliable method to calculate atomic charges on the basis of the total electron density only. It is based on a topological analysis of the total electron density to provide bond topological properties but also atomic properties like charges, volumes, and delocalization indexes used to find the bond order of the reactive surfaces delineating regions of charge concentration from charge depletion.[37] Q_{AIM} charges

dx.doi.org/10.1021/jp410301d | J. Phys. Chem. A 2013, 117, 14267−14275

were integrated for a promolecule using the VMoPro software.[19]

The charges on the two sulfur atoms are worth comparing. The S1 atom has three covalent bonds and has a positive topological Q_{AIM_EXP} charge of +0.50 e. The sulfonate S2 atom in the triflate anion is bonded to three oxygen atoms and has three fluorine atoms as its second neighbors. This position of S2 renders it highly deficient in electrons resulting in a net integrated Exp charge largely positive of +3.14 e. The three oxygen atoms display similar S−O bond lengths of 1.446 ± 0.004 Å. Their three atomic charges, which were not constrained to be equivalent in the Theo model, are similar. The cumulative negative Q_{AIM_EXP} charge on the three oxygen atoms riding on the S2 atom is −3.80 e (1.26 each as they were constraint to be equivalent), while that on the three fluorine atoms is −1.74 e.

The C15 atom holding the three fluorine atoms bears a large positive charge (Q_{AIM_EXP} = +1.41 e). For the two charge definitions and the two models this carbon atom is positively charged, while the fluorine atoms are negatively charged for all charge definitions.

Charge values of atoms in the triflate moiety are larger for the Q_{AIM} definition than for the Q_{val_κ} one.

In order to analyze the important role of the bromoethyl hydrogen atoms in the proposed mechanism, the charges of C13 and C14 atoms and those of their bonded hydrogen atoms deserve special attention. The C13 methylene CH_2 group was found to bear globally a slightly less positive charge compared to the C14 methylene for three out of the four charge types given in Table 6, presumably due to the presence of a bromine atom bound to C14 vs a sulfonium on the C13 atom. The relative acidity of H14(A,B) vs H13(A,B) atoms varies with the charges model considered.

The bromine atom is negatively charged in three charge models, except for Q_{VAL_κ}. The possible charge distribution of atoms mainly involved in the reaction mechanism represented in Scheme 5 is compatible with the same three types of charges.

Scheme 5. Distribution of Charges in Light of Charge Density Analysis

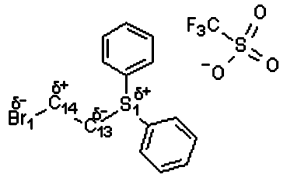

A refinement with the charges of the anion and cation not constrained to a formal unitary charge was also performed. The asymmetric unit having been kept neutral electrically during the refinement, the two ionic moieties necessarily hold complementary charges. The resulting model should reflect the ionic character of both molecules in the asymmetric unit. This is indeed the case; the triflate moiety turns out to be significantly negative as the sum of its atomic valence populations led to a total charge of −0.84 e in the Exp model, while the Theo charge of −0.62 e is more attenuated.

Electrostatic Potential. As the BEST compound is an ion pair, the triflate molecule has an overall negative electrostatic potential (ESP) and the bromoethyl biphenyl sulphonium moiety has an overall positive ESP. The electron density surface colored according to the ESP is shown in Figure 5. Globally, the Exp ESP shows larger values compared to the ESP derived from the Theo model. A large area of positive ESP is observed around the sulfonium group in both cases. The positive ESP generated by the sulfur atom is propagated toward the hydrogen atoms of the reactive bromoethyl group in the theoretical ESP.

The ESP issued from the Exp multipolar refinement is more positive around the two H14A,B hydrogen atoms (Figure 5) due to more positive charges on the hydrogen atoms and the bromine atom. The converse is observed for the theoretical model, where the potential is more positive around the H13A,B atoms due to the influence of the vicinal positive sulfonium atom. The electrostatic potential is much more electronegative in the theoretical model on the bromine atom compared to the experimental one.

The isosurface colored according to the ESP issued from the refinements without formal ±1e charge constraint on the cation/anion pair is shown in Figure Sup7, Supporting Information. The unconstrained Exp electrostatic potential is slightly attenuated compared to the constrained one, as the charge transfer between the ions is lower but qualitatively similar to the constrained one, notably around the bromoethyl group. The ESP from the theoretical unconstrained model is also attenuated except for the bromine atom and the region around which is far more electronegative.

Dipole Moment. The molecular dipole moments μ are calculated based on atomic net charges q_i derived from P_{val} and on the atomic dipoles μ_i (from the multipole formalism) according to the formula

$$\vec{\mu}_{Total} = \sum_i \vec{\mu}_i + \sum q_i \vec{r}_i$$

Due to the electroneutrality constraint which kept the total charge of the asymmetric unit equal to zero, μ is actually independent of the origin. Atomic dipole moment contributions are dependent on seven variables: the net charge derived from P_{val}, the atomic coordinates (corresponding to the location in space of atomic charges), and the three dipole populations P_{10}, P_{11+}, P_{11-}.

The BEST salt compound, being a polar entity, possesses relatively high dipole moment, which is found to be 25.2 and 28.8 D for the Exp and Theo models, respectively. Dipole moment vectors are shown in Figure 6 for both models. The system being composed of anionic and cationic molecules, the dipole moment orientation and magnitude are largely ruled by this property. Hence, the dipole moment vectors are roughly oriented in the direction joining the negative triflate moiety to the positive region located next to the C13−C14 group.

The dipolar charge distribution explaining the dipole moment orientation can also be seen on the electrostatic potential surfaces (Figure 6), with a negative potential around the triflate anion. The value of the dipole moment for the Exp model is found to be 15% lower than the theoretical one. If the formal charges of the two ions were not constrained to be ±1, the contrary would be observed, in accordance with the fact that molecular dipole moments derived from experimental charge density studies often present pronounced enhancements compared to independent theoretical estimates.[41]

■ CONCLUSION

An experimental charge density analysis of the compound bromoethyl sulfonium triflate was performed as well as a high-level ab initio periodic computation of the system. Analysis of

dx.doi.org/10.1021/jp410301d | J. Phys. Chem. A 2013, 117, 14267−14275

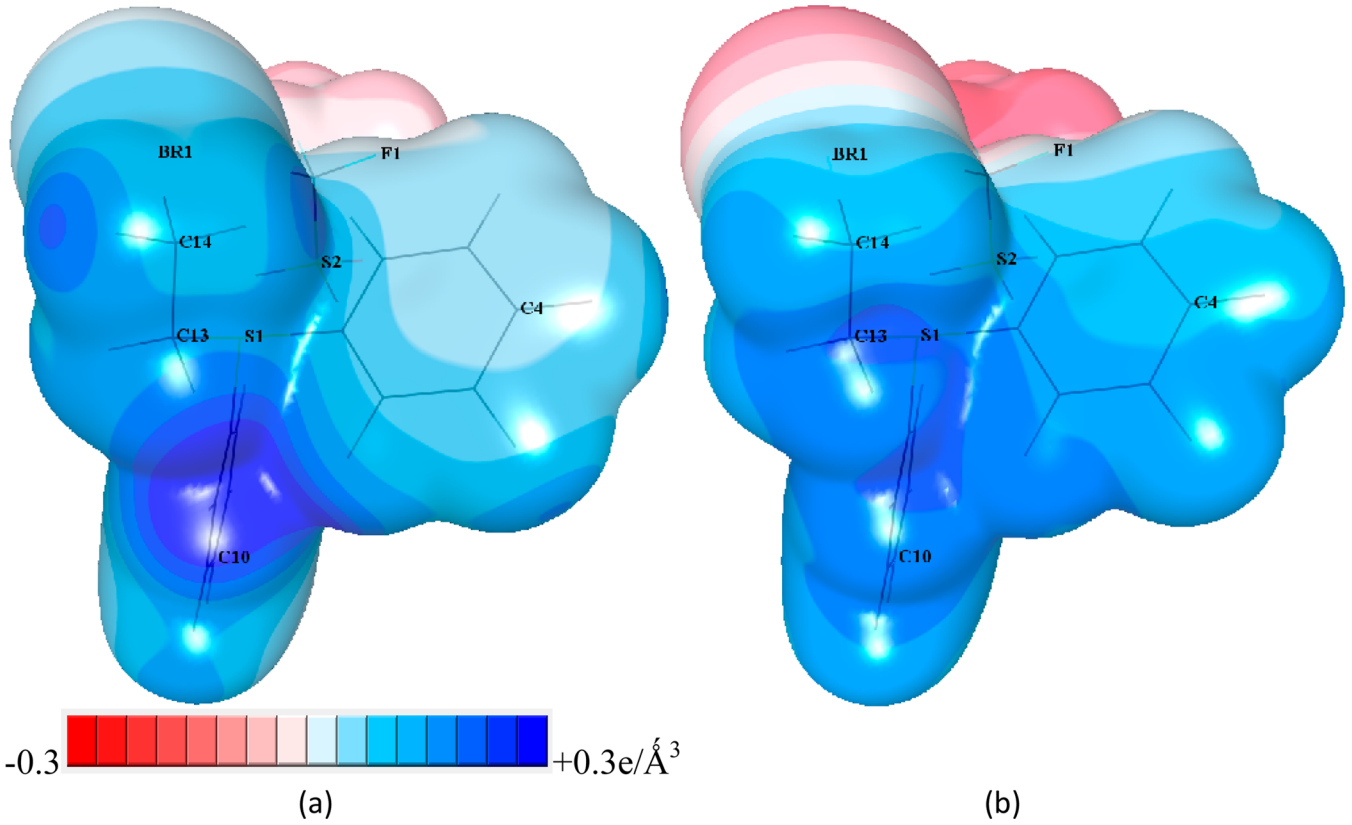

Figure 5. Isosurface of static total electron density at ρ = 0.01 e/Å^3 colored according to the electrostatic potential generated by the BEST promolecule. Bromoethyl sulfonium moiety is in the foreground, while the negatively charged triflate group is behind. View highlights the difference between the H atoms bound to C13 and C14 atoms. Properties are computed using (a) experimental data and (b) the theoretical multipolar model.

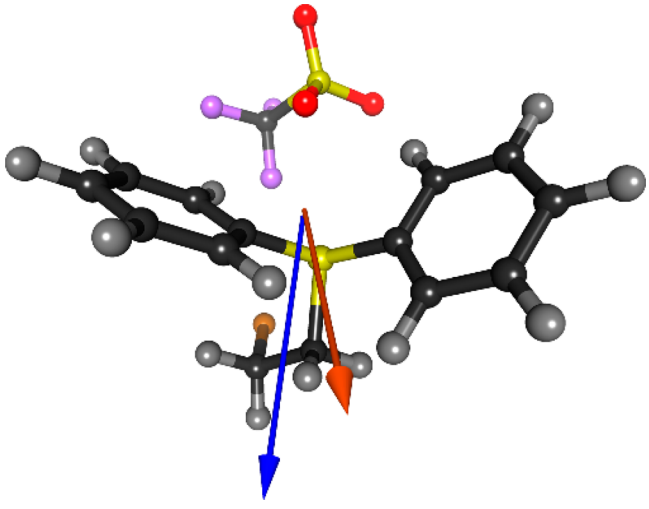

Figure 6. Total dipole moment for the BEST molecule computed from experimental (blue) and theoretical (red) models.

the charge distribution on the basis of the Exp model did reveal very interesting results.

Generally, it is believed that the C13 atom being attached to a triply covalently bonded S1$^+$ atom is comparatively more electron deficient. Thus, in this case, a base should preferentially abstract an acidic hydrogen from atom C13. The presence of the bromine atom adjacent to C14 renders the H14(A,B) hydrogen atoms also more acidic. The electrostatic potential at the molecular surface shows a strongly electropositive region around the sulfur atom, which is favorable to attract a nucleophile base. The electrostatic potential is also positive around the H14(A,B) hydrogen atoms compared to the H13(A,B) hydrogen atoms.

The distribution of charges raises again the question how the reaction actually proceeds. Previously, Yar et al.[4] indentified the in situ transformation of the bromoethyl sulfonium salt to vinyl sulfonium salt in the presence of a base. In this process, a base removes a proton from a carbon atom of the bromoethyl group and then an elimination reaction occurs (the HBr group being removed).

The question raised by our study is whether the proton is removed from the C14 or C13 atom. Most likely if H$^+$ is removed from the C13, which is adjacent to the positively charged S1 atom, the carbanion would be more stable than if the proton is taken from the C14 atom, located next to the bromine atom.

A possibility remains that proton extraction occurs first on C14, which holds more acidic hydrogen atoms according to the experimental electrostatic potential map. Then, the relative stability of the C14 and C13 carbanions being in favor of the second one, the C14 atom may be reprotonated by exchange with the neighbor atom C13. At this point, the C13 carbanion being stabilized by the S1$^+$ atom, no reverse protonation would take place. In particular, a possible perspective would be to analyze, in the same way, what the DVST vinyl homologue is producing in situ (Scheme 2).

dx.doi.org/10.1021/jp410301d | J. Phys. Chem. A 2013, 117, 14267−14275

■ ASSOCIATED CONTENT

Supporting Information

Plot of observed vs expected residual electron density; plot of average F_{obs}/average F_{calcd}, residual and static electron density maps; R_{free} plotted as a function of restraints weight; Hirshfeld surface; fingerprint plots of the Hirshfeld surface; molecular surface colored according to ESP after refinement without formal charge constraint on anion/cation; list of bond and intermolecular critical points with topological properties This material is available free of charge via the Internet at http://pubs.acs.org.

■ AUTHOR INFORMATION

Corresponding Author

*E-mail: christian.jelsch@univ-lorraine.fr.

Notes

The authors declare no competing financial interest.

■ ACKNOWLEDGMENTS

M.A. thanks the Higher Education Commission of Pakistan for Ph.D. funding.

■ REFERENCES

(1) Unthank, M. G.; Hussain, N.; Aggarwal, V. K. *Angew. Chem., Int. Ed.* **2006**, *45*, 7066.
(2) Kokotos, C. G.; McGarrigle, E. M.; Aggarwal, V. K. *Synlett* **2008**, *2008*, 2191.
(3) Yar, M.; McGarrigle, E. M.; Aggarwal, V. K. *Angew. Chem., Int. Ed.* **2008**, *47*, 3784.
(4) Yar, M.; McGarrigle, E. M.; Aggarwal, V. K. *Org. Lett.* **2009**, *11*, 257.
(5) Yar, M.; Unthank, M. G.; McGarrigle, E. M.; Aggarwal, V. K. *Chem.—Asian J.* **2011**, *6*, 372.
(6) Fritz, S. P.; Mumtaz, A.; Yar, M.; McGarrigle, E. M.; Aggarwal, V. K. *Eur. J. Org. Chem.* **2011**, *2011*, 3156.
(7) McGarrigle, E. M.; Fritz, S. P.; Favereau, L.; Yar, M.; Aggarwal, V. K. *Org. Lett.* **2011**, *13*, 3060.
(8) von E. Doering, W.; Schreiber, K. C. *J. Am. Chem. Soc.* **1955**, *77*, 514.
(9) Wang, Y.; Zhang, W.; Colandrea, V. J.; Jimenez, L. S. *Tetrahedron* **1999**, *55*, 10659.
(10) Gosselck, J.; Béress, L.; Schenk, H. *Angew. Chem., Int. Ed. Engl.* **1966**, *5*, 596.
(11) Wijtmans, R.; Vink, M. K. S.; Schoemaker, H. E.; van Delft, F. L.; Blaauw, R. H.; Rutjes, F. P. J. T. *Synthesis* **2004**, *2004*, 641.
(12) Yar, M.; McGarrigle, E. M.; Aggarwal, V. K. In *Encyclopedia of Reagents for Organic Synthesis*; John Wiley and Sons Ltd.: New York, 2012.
(13) *Agilent*; Agilent Technologies Ltd.: Yarnton, England, 2010.
(14) Clark, R. C.; Reid, J. S. *Acta Crystallogr., Sect. A* **1995**, *51*, 887.
(15) Blessing, R. H. *Crystallogr. Rev.* **1987**, *1*, 3.
(16) Zhurov, V. V.; Zhurova, E. A.; Pinkerton, A. A. *J. Appl. Crystallogr.* **2008**, *41*, 340.
(17) Altomare, A.; Cascarano, G.; Giacovazzo, C.; Guagliardi, A. *J. Appl. Crystallogr.* **1993**, *26*, 343.
(18) Sheldrick, G. *Acta Crystallogr., Sect. A* **2008**, *64*, 112.
(19) Jelsch, C.; Guillot, B.; Lagoutte, A.; Lecomte, C. *J. Appl. Crystallogr.* **2005**, *38*, 38.
(20) Hansen, N. K.; Coppens, P. *Acta Crystallogr.* **1978**, *A34*, 909.
(21) Allen, F. *Acta Crystallogr., Sect. B* **1986**, *42*, 515.
(22) Farrugia, L. *J. Appl. Crystallogr.* **1997**, *30*, 565.
(23) Dovesi, R.; V. R. S.; Roetti, C.; Orlando, R.; Zicovich-Wilson, C. M.; Pascale, F.; Civalleri, B.; Doll, K.; Harrison, N. M.; Bush, I. J.; D'Arco, P.; Llunell, M. *DFT*, Version 1_0_2; University of Turin: Italy, 2008.
(24) Hohenberg, P.; Kohn, W. *Phys. Rev.* **1964**, *136*, 864.
(25) Lee, C.; Yang, W.; Parr, R. G. *Phys. Rev. B* **1988**, *37*, 785.
(26) Becke, A. D. *J. Chem. Phys.* **1993**, *98*, 5648.
(27) Hariharan, P. C.; Pople, J. A. *Theor. Chim. Acta* **1973**, *28*, 213.
(28) Le Page, Y.; Gabe, E. J. *Acta Crystallogr.* **1979**, *A35*, 73−78.
(29) Madsen, A. *J. Appl. Crystallogr.* **2006**, *39*, 757.
(30) Stewart, R. *Acta Crystallogr.* **1976**, *A32*, 565.
(31) Zarychta, B.; Zaleski, J.; Kyziol, J.; Daszkiewicz, Z.; Jelsch, C. *Acta Crystallogr., Sect. B* **2011**, *67*, 250.
(32) Pillet, S.; Souhassou, M.; Lecomte, C.; Schwarz, K.; Blaha, P.; Rérat, M.; Lichanot, A.; Roversi, P. *Acta Crystallogr., Sect. A* **2001**, *57*, 290−303.
(33) Coppens, P.; Guru Row, T. N.; Leung, P.; Stevens, E. D.; Becker, P. J.; Yang, Y. W. *Acta Crystallogr., Sect. A* **1979**, *35*, 63.
(34) Mette S. Schmøkel, M. S.; Cenedese, S.; Overgaard, J.; Jørgensen, M. R. V.; Chen, Y.-S.; Gatti, C.; Stalke, D.; Iversen, B. B. *Inorg. Chem.* **2012**, *51*, 8607−8616.
(35) Love, I. *J. Phys. Chem.* **2009**, *113*, 2640−2646.
(36) Love, I. *J. Phys. Chem.* **2006**, *110*, 10507−10512.
(37) Bader, R. F. W. *International Series of Monographs on Chemistry*, 1st ed.; Clarendon Press: Oxford, U.K, 1990; Vol. *22*.
(38) McKinnon, J. J.; Spackman, M. A.; Mitchell, A. S. *Acta Crystallogr., Sect. B* **2004**, *60*, 627.
(39) McKinnon, J. J.; Jayatilaka, D.; Spackman, M. A. *Chem. Commun.* **2007**, 3814.
(40) Desiraju, G. R.; Steiner, T. *IUCr Monographs on Crystallography*; Oxford: Oxford University Press/IUCr, 1999; , Vol. *9* (The weak hydrogen bond in structural chemistry and biology).
(41) Spackman, M. A..; Munshi, P..; Dittrich, B. *Chem. Phys. Chem.* **2007**, *8*, 2051.